Sorption of Phenyl Mercury, Methyl Mercury, and Inorganic Mercury onto Chitosan and Barbital Immobilized Chitosan: Spectroscopic, Potentiometric, Kinetic, Equilibrium, and Selective Desorption Studies

S. Kushwaha,[†] B. Sreedhar,[‡] and P. Padmaja*[,†]

Department of Chemistry, Faculty of Science, The M. S. University of Baroda, Vadodara, India, and Department of Inorganic & Physical Chemistry, Indian Institute of Chemical Technology, Hyderabad, India

The objective of the study was to elucidate the binding of Hg^{2+}, methyl mercury, and phenyl mercury on chitosan and barbital-immobilized chitosan by potentiometric titration and XPS and FTIR spectroscopy. Adsorption experiments were conducted at room temperature (30 °C) to optimize the percentage removal of different forms of mercury, and the data were fitted to Langmuir and Freundlich adsorption isotherms. Speciation of inorganic, methyl, and phenyl mercury was achieved by sequentially eluting inorganic mercury using 0.1 N perchloric acid followed by methyl mercury using 0.015 N NaCl and finally phenyl mercury using 0.05 N EDTA. Potentiometric titration data and a pK_a spectrum approach showed the presence of self-assembled amine/protonated amine, amine, and hydroxyl/amine functional groups. The total number of functional groups was found to be 158.05 mol·g^{-1} and 68.6 mol·g^{-1} for barbital-immobilized chitosan and chitosan, respectively, suggesting that a larger number of binding sites are available in barbital-immobilized chitosan for bonding to mercury. FTIR, pH, and XPS studies show that the possible functional groups in the metal binding include amino functional groups in the case of chitosan and amide groups in the case of barbital-immobilized chitosan. The peak areas of XPS Hg 4f spectra show greater adsorption for Hg using barbital-immobilized chitosan as adsorbent compared to chitosan.

Introduction

Mercury is generally considered to be one of the most toxic metals found in the environment. The major sources of mercury pollution in the environment are industries such as chloralkali, paints, pulp and paper, oil refining, rubber processing, fertilizer, batteries, thermometers, fluorescent light tubes, high intensity street lamps, pesticides, cosmetics, and pharmaceuticals.[1] Cost-effective technologies to remove mercury from the waste streams are sought. Conventional methods used are the electrolysis reduction process, sulfide precipitation, ion exchange, alum and iron coagulation, and adsorption on activated carbon.[2,3] Biosorption has also been recognized as an effective method for the reduction of metal contamination in surface water and in industrial effluents. Recently, a number of nonconventional adsorbents have been used for removal of mercury from wastewater.[4−9] Among these, chitosan, a biopolymer, has been used as a promising adsorbent.

Chitosan is a linear polysaccharide composed of β (1→4) linked 2-amino-2-deoxy-D-glucose and 2-acetamido-2-deoxy-D-glucose units. It is biodegradable and has gelling ability, and its properties can be further modified by derivatization of its amino and hydroxyl groups. Chitosan and its derivatives have been used for removal of metal ions from wastewater.[10−20] The suitability of chitosan and cross-linked chitosan have been studied for adsorption of mercury.[13,14] Elemental mercury removal on chitosan, iodine (bromide), or sulfuric acid-modified chitosan has been studied.[12] Limited reports exist in the literature on the removal of methyl mercury and phenyl mercury using chitosan as an adsorbent. Methyl mercury adsorption has been studied using chitosan as an adsorbent in a column.[10] Also surface modification has become a common technique in providing a material with desirable functional properties. Several investigations were done to modify chitosan to facilitate mass transfer and to expose the binding sites to enhance the adsorption capacity.[21] Chitosan and chitosan-grafted polyacrylamide beads and thiol-modified chitosan have been reported for the adsorption of inorganic mercury.[11,22]

Most of the studies have been done to optimize sorption performance, especially sorption isotherms, with some suggesting uptake mechanisms, but little has been done on the identification of the sorption sites and interpretation of the molecular interactions between sorbent and solute by XPS analysis and mechanistic modeling using potentiometric titrations.[23,24] The ability of mercury(II) to form a complex with barbital (5,5-diethylbarbituric acid) has been used as the basis for the separation and determination of barbiturates where barbital was treated with excess mercury(II) to form a chloroform extractable complex.[25] Advantage was taken of the ability of mercury to form a mercury−barbital complex for the determination of mercury.[26] This suggested that more detailed study could be done to find the suitability of grafting barbital onto chitosan and use of it as an adsorbent for the removal of inorganic, methyl, and phenyl mercury. In this work, chitosan and barbital-grafted chitosan were evaluated for the removal of inorganic mercury (Hg^{2+}), methyl mercury (CH_3Hg), and phenyl mercury (PhHg), and parameters were optimized for their maximum removal. The possibility of speciation of inorganic, methyl, and phenyl mercury was explored using 0.1 N perchloric acid, 0.9 % NaCl, and 0.05 N EDTA. Detailed studies using

* To whom correspondence should be addressed. E-mail: p_padmaja2001@yahoo.com.
[†] The M. S. University of Baroda.
[‡] Indian Institute of Chemical Technology.

10.1021/je100317t © 2010 American Chemical Society
Published on Web 09/14/2010

spectroscopic and potentiometric techniques on the adsorption of different forms of mercury onto chitosan and barbital-immobilized chitosan and their kinetics, thermodynamics, and speciation have been reported for the first time.

Materials and Methods

Sorbent Preparation. Chitosan flakes (87.6 % deacetylated and molecular weight $5.5 \cdot 10^5$ g/mol) from Sigma-Aldrich were used to prepare chitosan beads. One % (w/w) chitosan solution was prepared by dissolving chitosan flakes in 1 % (w/w) acetic acid solution at room temperature for homogenizing the mixture for 48 h. The homogeneous chitosan solution was injected dropwise into 0.41 N NaOH solution for the formation of beads. After the formation of beads, it was stored overnight in a freezer for hardening (Scheme S1, Supporting Information). The beads were extensively washed with distilled water until neutral and then used for the preparation of barbital-grafted chitosan and for further experimental studies as adsorbent (C). For the preparation of barbital-grafted chitosan [BC] (Scheme S1), a solution of neutralized beads of chitosan with 1 % sodium barbiturate (dissolved in double distilled water) in a ratio of 1:1 was stirred for 24 h at 50 °C, filtered, washed with double-distilled water until neutral, and then air-dried.

Batch Adsorption Experiments. Experiments were conducted to study the effect of various parameters for the removal of inorganic, methyl, and phenyl mercury on C and BC at 30 °C. For each experiment, 25 mL of Hg^{2+} solution of known initial concentration and pH were taken in a 100 mL stoppered conical flask. A suitable adsorbent dose was added to the solution, and the mixture was shaken at a constant speed. The supernatant was separated from the adsorbent by filtration and analyzed for the presence of unadsorbed Hg^{2+} by CVAAS (MA-5840 analyzer ECIL). All the experiments were conducted in triplicate, and the average results are reported. The mercury uptake by chitosan was calculated as follows:

$$q_e = (C_i - C_e)/m \quad (1)$$

where C_i is the initial concentration of metal ion $mg \cdot L^{-1}$, C_e is the equilibrium concentration of metal ion ($mg \cdot L^{-1}$), m is the mass of adsorbent ($g \cdot L^{-1}$), and q_e is the amount of metal ion adsorbed per gram of adsorbent. The experiments performed without adsorbent were treated as blanks.

Desorption. Sequential desorption studies were carried out using different eluents for the speciation study of mercury and methyl and phenyl mercuric acetate. A 0.2 g amount of inorganic, methyl, or phenyl mercury (0.8 mg/mL)-loaded adsorbent was added to 10 mL of eluent solution, and the pH was varied using 0.1 N HNO_3 or NaOH. The flasks containing solutions were shaken in a shaker for 10 min at 180 rpm. The supernatant was separated from the adsorbent by filtration and analyzed for the presence of desorbed mercury.

Fourier Transform Infrared Spectroscopy. Spectra for biosorbent and the metal-loaded biosorbents were obtained using a Perkin-Elmer RX1 model within the wavenumber range of (400 to 4000) cm^{-1}. Specimens of samples were first mixed with KBr and then ground in a mortar at an appropriate ratio of 1/100 for the preparation of the pellets. The resulting mixture was pressed at 10 tons for 5 min, and 16 scans with 8 cm^{-1} resolution were applied to record spectra. The background obtained from the scan of pure KBr was automatically subtracted from the sample spectra.

X-ray Photoelectron Spectroscopic Analysis. The surface of the samples was analyzed using a KRATOS AXIS 165 X-ray photoelectron spectrometer as reported elsewhere.[27]

Potentiometric Titration and Data Analysis. Potentiometric experiments were carried out according to a given procedure.[28] An adsorbent mass of 0.1 g was suspended in 50 mL of 0.01 N KNO_3 solution, and the suspension was purged with N_2 for 30 min to dissipate CO_2 and then left for 24 h to equilibrate the solution in electrolyte. The suspensions were acidified to pH 3.5 using 0.1 N HNO_3 and then titrated to pH 11 using 0.1 N NaOH. All experiments were conducted in triplicate in a glass vessel with a lid as part of a Spectralab AT-38C automatic potentiometric titrator. The temperature was recorded with a temperature sensor; the error of the temperature probe was ± 0.1 °C. The pH electrode was three-point calibrated with buffers (pH 4, 7, and 10) before each experiment, and the slope did not deviate more than 1 % from the Nernst value. The titrator unit was programmed with a step volume dose mode for the titration, which adds 0.001 mL of titration solution according to the pH changes.

The titration data were analyzed using the linear programming method (LPM) approach or so-called pK_a spectrum method as proposed by Brassard[29] and applied to bacterial suspensions as described by Cox, Dittrich, and Skolov.[30−32] The matrices used to solve the linear programming problem were set up as in the Brassard report and solved using a Matlab linear programming routine.

Results and Discussion

Uptake Studies. The effect of pH on the adsorption of inorganic, methyl, and phenyl mercury by C/BC was studied by varying the solution pH over a range of 1 to 8 using 0.1 N $NaOH/HNO_3$. A large number of binding sites exist on C and BC such as amine, amide, and hydroxyl groups. The nitrogen atom of the amino group and oxygen atoms of the hydroxyl groups can bind to a proton or a metal ion by electron pair sharing. The electronegativity of oxygen being more than that of nitrogen, the donation of a lone pair of electrons from the nitrogen atom will be more facile than the oxygen atom for bond formation with mercury. In the case of chitosan under highly acidic conditions (pH 1 to 2), there was no sorption of mercury because the binding sites are protonated which causes repulsion of the approaching mercury cation. As pH increases (3 to 7), the sorption of mercury increases because electron-rich binding sites are exposed which allow metal ion binding to the biosorbent.[33]

Beyond pH 7, sorption decreases due to precipitation as shown in Figure 1. At low and high pH, hydrogen bonding can also result between metal/mercuric hydroxide and the hydroxyl groups of C and BC. So the total uptake of mercury could be by electrostatic attraction, hydrogen bonding, and weak van der Waals forces.

$$R\text{-}NH_2 + H^+ \leftrightarrow R\text{-}NH_3^+$$

$$R\text{-}NH_2 + Hg^{2+} \rightarrow R\text{-}NH_2Hg^{2+}$$

$$R\text{-}NH_3^+ + Hg^{2+} \rightarrow R\text{-}NH_2Hg^{2+} + H^+$$

In BC, which has an amide group, both C−N and C−O bonds possess comparable amounts of single and double bond character, resulting in considerable delocalization of negative charge on the amide carbonyl oxygen atom causing predominant proton−metal ion interactions. As the pH increases, the hydroxyl groups become deprotonated, resulting in negative charge

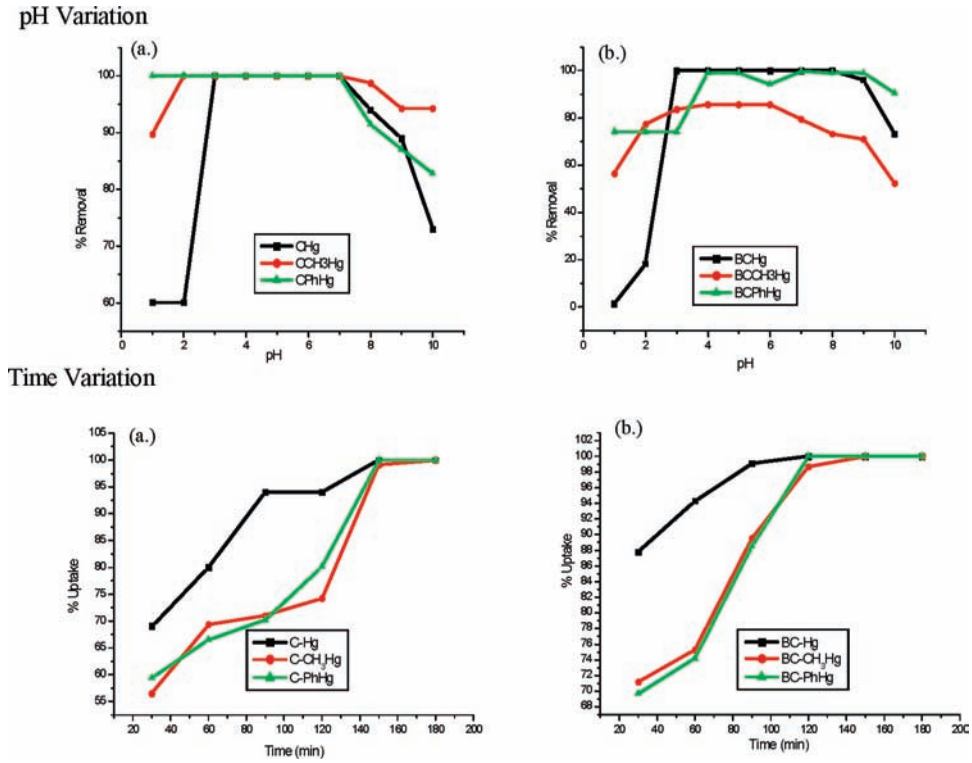

Figure 1. Effect of pH and time on uptake: (a) chitosan; (b) barbital-immobilized chitosan.

$$\text{R-OH} + \text{OH}^- \leftrightarrow \text{R-O}^- + \text{H}_2\text{O}$$

$$\text{R}'\text{-O}^- + \text{Hg}^{2+} \leftrightarrow \text{R}'\text{-O-Hg}^+$$

Thus, due to stronger electrostatic attraction between the lone pairs of the nitrogen atom and Hg^{2+} and also the electrostatic attraction between the negatively charged hydroxyl group and positive or neutral mercury species, adsorption occurs in the pH range 3 to 7. The adsorption of Hg^{2+} at low pH values for C was found to be comparatively higher than that for BC due to strong electrostatic attraction between the lone pair of nitrogen and Hg^{2+} species rather than the competing protons. The adsorption is higher in the case of BC with a concomitant increase in pH values due to deprotonation of amide groups and formation of covalent bonds between O, N, and Hg.

An uptake study with respect to time (Table S1) showed 100 % uptake after 3 h for C, whereas BC shows full uptake after 2 h. Hg^{2+} was found to adsorb at a faster rate with higher percentage removal than organic mercury ions. Since the mercury(II) ion has a smaller ionic radius, it is possible that mercury(II) ions diffuse faster through the adsorbent pores than the bulkier organic mercury. Similarly, temperature studies (Table S1) showed that adsorption on C is endothermic whereas it is exothermic in the case of BC. The increase in mercury adsorption with increasing temperature might be due to an enhanced rate of intraparticle diffusion of the adsorbate, as diffusion is an endothermic process.

Biosorption Isotherms. The adsorptive capacity of C and BC used for mercury removal was determined through adsorption isotherm studies. The Langmuir and Freundlich models were used to determine the adsorption capacity of mercury on C and BC (Table S2 and Figure 2). From the coefficient of determination values (r^2) obtained for the two models, it can be seen that the Langmuir and Freundlich models cannot be applied to these data. A similar behavior was observed by Gregory et al. during the study of Cd^{2+} ions on porous magnetic chitosan beads.[34] This suggests that mercury ions penetrate the adsorbent and adsorb onto amine/amide sites and metal clusters form, which might block the pores. This renders the active sites lying in the interior inaccessible for adsorption.

Adsorption Dynamics. The objective of an adsorption kinetic study is to investigate the possible mechanism for the sorption process and to determine the time required to achieve equilibrium. Kinetics was examined for the sorption of Hg^{2+}, CH_3Hg^{2+}, and $PhHg^{2+}$ on both C and BC using a series of measurements extending from 30 to 240 min at 25 °C (Table S2 and Figure 3). The rate of adsorption is fast for both adsorbents in the case of Hg^{2+}, CH_3Hg^{2+}, and $C_6H_5Hg^{2+}$. However, the time needed to attain equilibrium is longer when using C (160 min) rather than BC (120 min). This could be explained by the presence of a larger number of functional groups for bonding in the case of BC (potentiometric titrations). However, Hg^{2+} adsorbed at a faster rate, followed by CH_3Hg^{2+} and $C_6H_5Hg^{2+}$. This could be due to the smaller ionic radius of Hg^{2+} which enables it to diffuse faster than the bulkier $C_6H_5Hg^{2+}$ and CH_3Hg^{2+}. More than 99 % of the total mercury was removed within a period of 160 min. This rapid initial binding rate suggests an instantaneous binding of mercury on surface sites followed by slower and nonspecific binding to other components.

In order to investigate the adsorption process of Hg^{2+}, CH_3Hg^{2+}, $C_6H_5Hg^{2+}$, three kinetic models were used: the pseudo-first-order rate equation, pseudo-second-order rate equation, and intraparticle diffusion equation.

Pseudo-First-Order Model. The sorption kinetics can be defined by a pseudo-first-order model.

$$\mathrm{d}q/\mathrm{d}t = K_1'(q_e - q_t) \qquad (2)$$

where q_e is the amount of solute adsorbed at equilibrium per unit weight of adsorbent ($mg \cdot g^{-1}$), q_t is the amount of solute adsorbed at any time ($mg \cdot g^{-1}$), K_1' is the adsorption constant, and the equation can be linearized as a function of time.

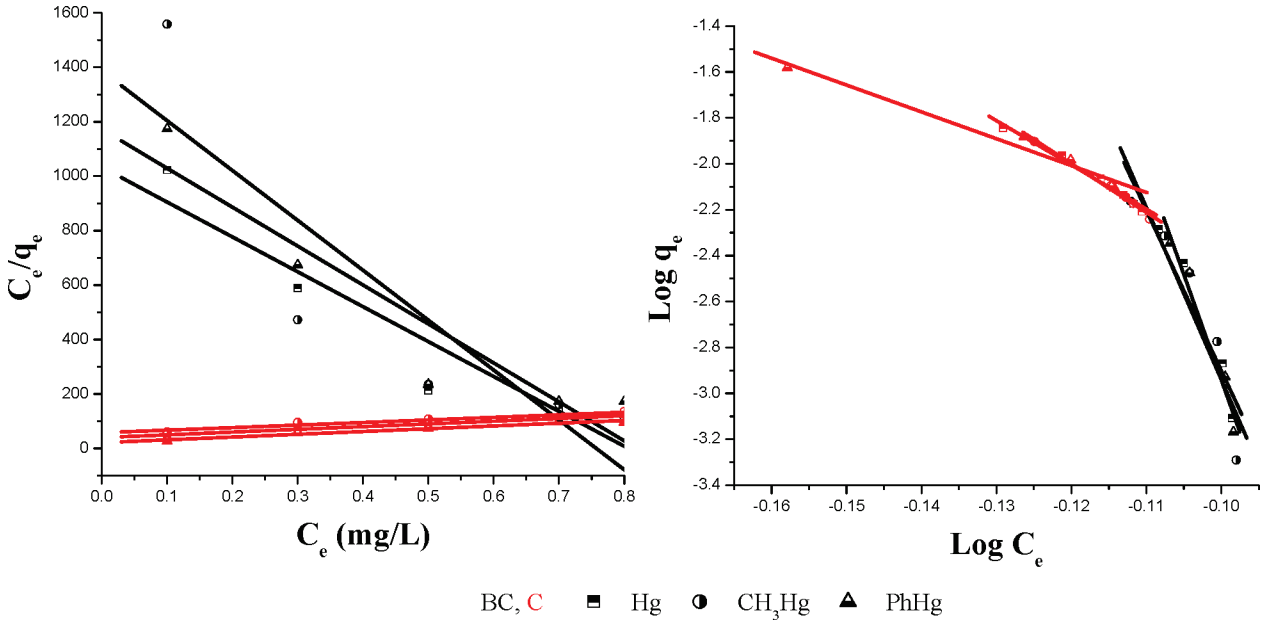

Figure 2. Freundlich and Langmuir isotherm plots for C and BC.

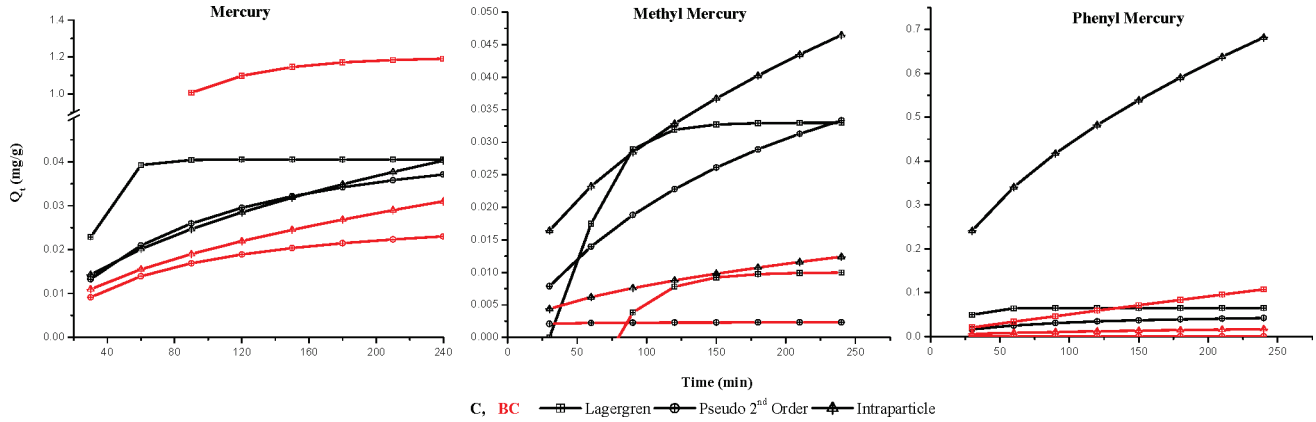

Figure 3. Different kinetic plots for C and BC.

$$\log(q_e - q_t) = \log q_e - K_1' t/2.303 \quad (3)$$

Plots for the linearized equation were constructed, and the constants were calculated from the slopes and intercepts of the plots of $\log(q_e - q_t)$ vs time. Correlation coefficient values were low, and the calculated q_e values did not agree with the experimental q_e values. This suggests that the adsorption of all forms of mercury does not follow pseudo-first-order kinetics.

Pseudo-Second-Order Model. This model is based on the solid capacity and has been presented for the kinetics of sorption of divalent metal ions.

$$q_t = q_e^2 K_2' t/(1 + q_e K_t) \quad (4)$$

where K_2' is the pseudo-second-order rate constant (g·mg^{-1} min). The above equation can be rearranged to obtain the linearized form which is shown as follows:

$$t/q_t = 1/q_e^2 K_2' + t/q_e \quad (5)$$

The pseudo-second-order constants K_2' and can be determined experimentally by plotting t/q_t vs t. The plots show that correlation coefficients of the second-order kinetic model obtained were much less, indicating that the adsorption process does not obey the pseudo-second-order kinetic model.

Intraprticle Diffusion Study. The equation for the Weber−Morris intraparticle diffusion model is:

$$q_t = K_i t^{0.5} \quad (6)$$

where k_i is the intraparticle diffusion rate constant (mg·g^{-1} min$^{0.5}$). Correlation coefficients for all the plots were found to be > 0.97, suggesting pore-controlled diffusion.

Desorption. Desorption[35] studies were carried out using different eluents for mercury and methyl and phenyl mercuric acetate (Figure 4). Inorganic mercury was eluted quantitatively using 0.1 N perchloric acid while phenyl and methyl mercury were not eluted at all. Methyl mercury was eluted quantitatively using 0.015 N NaCl while phenyl mercury was not eluted with NaCl. Phenyl mercuric acetate was quantitatively eluted using 0.05 N EDTA. Advantage was taken of these observations and sequential desorption was achieved by first eluting inorganic mercury using 0.1 N perchloric acid followed by methyl mercury using 0.015 N NaCl and finally phenyl mercury using 0.05 N EDTA.

FTIR Spectroscopy. Typical absorption frequencies of infrared spectra of the chitosan, BC, and mercury-loaded species

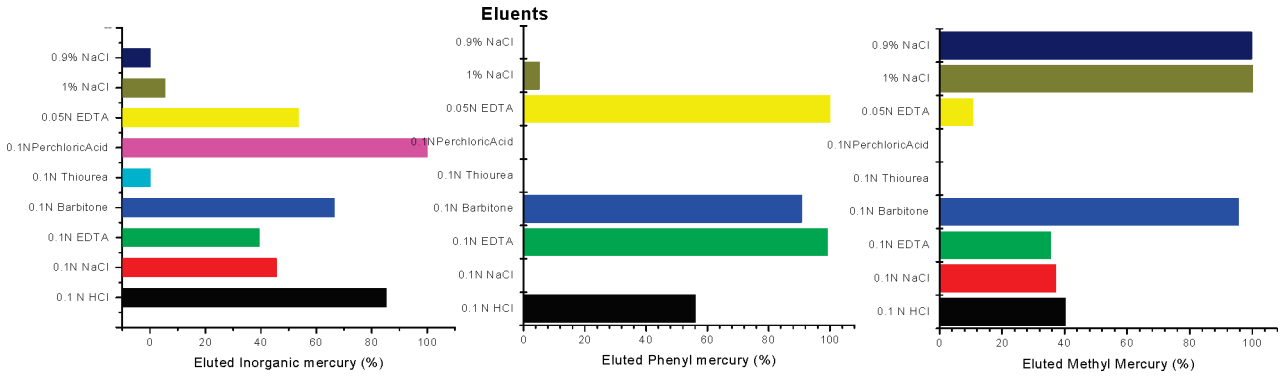

Figure 4. Desorption of inorganic and organic mercury using a number of eluents.

Table 1. Typical Absorption Frequencies of Infrared Spectra of the C and BC

wave numbers (cm^{-1})						
C	C-Hg	C-CH_3Hg	C-PhHg	range	intensity	assignment
3447.7	3432.7	3445.06	3441.3	3300 to 3500	strong	N−H and OH stretching
2929.7	2920.1	2921.4	2921.4	2700 to 2950	variable	C−H stretching
1632.3	1599.4	1597.93	1597.38	1400 to 1640	variable	N−H bending
1383.8	1384.1	1383.69	1383.61	1280 to 1430	variable	C−H bending
1074.6	1086.2	1089.77	1090.1	900 to 1380	variable	C−N, C−O stretch
wave numbers (cm^{-1})						
BC	BC-Hg	BC-CH_3Hg	BC-PhHg	range	intensity	assignment
3425.7	3449.0	3432.5	3434.9	3300 to 3500	strong	N−H and OH stretching
2924.6	2924.0	2924.04	2923.1	2700 to 2950	variable	C−H stretching
1654.3	1636.7	1636.7	1637.97	1620 to 1725	variable	C═O stretching
1560.2	1512.9	1511.2	1508.9	1400 to 1640	variable	N−H bending
1380.3	1384.0	1384.05	1382.8	1280 to 1430	variable	C−H bending
1073.9	1077.5	1024.05	1080.3	900 to 1380	variable	C−N, C−O stretch

with their corresponding assignments are summarized in Table 1. The strong broad band in the region of (3300 to 3500) cm^{-1} is characteristic of the N−H stretching vibration although there is the possibility of overlap between the N−H and the O−H stretching vibrations in C/BC. Frequencies for N−H stretching and bending were found to decrease after mercury adsorption in the case of C and BC, showing the bonding of Hg^{2+} with the N of amine where the lone pair of electrons of the nitrogen atom was donated to the shared bond between the N and Hg^{2+} and, as a consequence, the electron cloud density of the nitrogen atom was reduced, causing the shift. For BC, the FTIR spectrum shows a peak at 1654 cm^{-1} specifically for the amide groups, indicating the grafting of barbital on chitosan. The amide stretching frequency shifts from 1654 cm^{-1} to a lower frequency of 1636 cm^{-1} after mercury adsorption, showing the possible interaction of metal linkage with O and N of the amide group.[36] Mercury adsorption is found to affect the frequencies of all the bonds with the N atoms of the amine and amide, indicating that nitrogen atoms (amine group) are the main adsorption sites for mercury adsorption on C while in the case of BC it is N and O (amide and amine group).

XPS Analysis. Typical wide scan XPS spectra for chitosan and its derivative before and after mercury adsorption are shown in Figure 5.

In addition to binding energy peaks at 284.61 eV for C1S, (532.6 and 532.03) eV for O1S, and 398.52 eV for N1S in chitosan, there are no additional peaks observed in BC, except for lowering of binding energy of the N1S peak in BC. This lowering of binding energy of the N1S peak suggests that nitrogen atoms are more electron rich due to formation of a NH−CO−NH linkage, and intensification of C1S and N1S peaks suggests that barbital was immobilized on chitosan.

The presence of mercury on the surface of C and BC is obvious after the adsorption experiment. The wide scan clearly shows a small peak around 101.5 eV after the mercury biosorption onto the prepared sorbents, indicating the accumulation of mercury on the sorbents.[37]

After mercury adsorption, there is a peak at a binding energy of about 399.5 eV for N1S in the case of chitosan which can be attributed to the N atom in the R-NH_2 group.[38] After adsorption, a shift in the N1S peak is observed at a binding energy greater than 399.5 eV in the case of Hg^{2+} and methyl mercury. This can be attributed to the formation of a Hg−NH_2 complex in which a lone pair of electrons in the nitrogen atom is shared between the N and Hg^{2+} and, as a consequence, the electron cloud density of the nitrogen atom is reduced, resulting in the higher binding energy peak observed. But a much less intense peak was observed at increased BE, indicating the limited amount of the R-NH_2−Hg^{2+} complex.[3940,41] However, in the case of phenyl mercury the peak is at a lower energy, suggesting the interaction to be nonspecific electrostatic. In the case of BC after adsorption of all three species of mercury, two peaks were observed in the N1S spectrum. The new peaks at 398.53 eV, 398.81 eV, and 398.88 eV for Hg^{2+}, CH_3Hg^{2+}, and $C_6H_5Hg^{2+}$, respectively, indicate that many nitrogen atoms in BC are in a more reduced state due to metal adsorption.

The XPS spectrum of Hg 4f level (4f7/2 and 4f5/2) is shown in Figure S1. The Hg 4f spectrum shows two peaks with binding energies 101.52 eV and ∼ 105 eV in agreement with the difference in the energy predicted by spin orbit splitting. The intensity of the Hg 4f5/2 peak is seen to change though the amount of sorbed Hg analyzed from the solution remained constant in each case. The spatial distribution of mercury could be different, leading to the changes in intensities observed. It is shown in Figure S1 that the peak area of Hg 4f in the mercury-loaded BC is larger than that in the mercury-loaded C, reflecting the higher mercury sorption capacity of the BC. This is

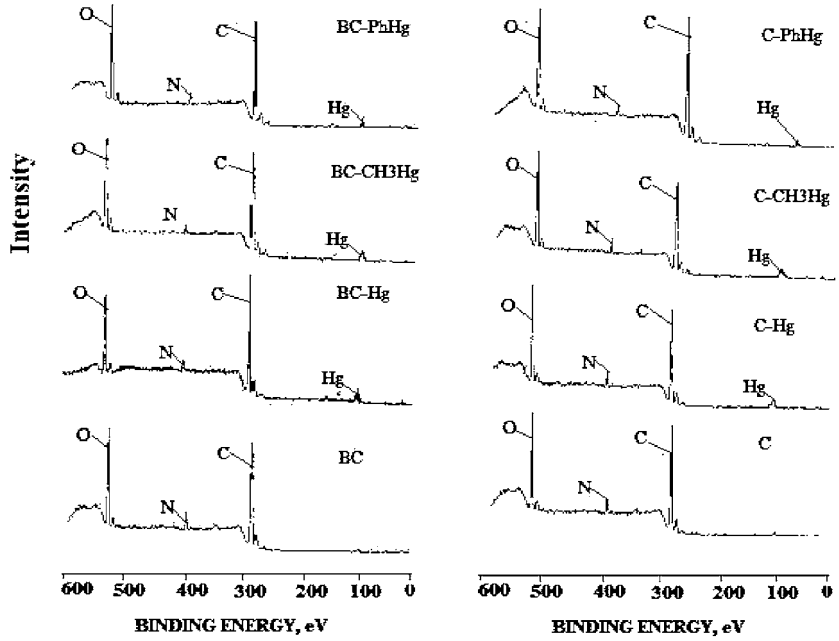

Figure 5. Typical wide-scan XPS spectra of metal-loaded and unloaded C and BC.

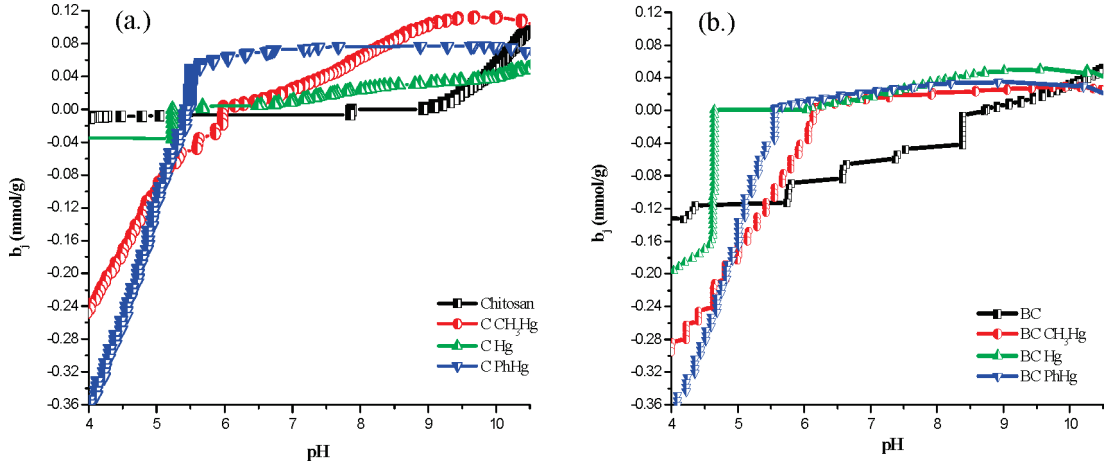

Figure 6. Potentiometric titration of (a) C and C with metal ions and (b) BC and BC with metal ions.

consistent with the observations in both the sorption isotherm and pH effect experiments.

Data Analysis. Results of potentiometric titration curves are used to generate a simplified mathematical model using Matlab.[29−32] It can be found that the adsorbent features several pK_a values. From Figure 6 it can be seen that C has a higher capacity of neutralizing hydroxide ions whereas BC has a slightly lower capacity for neutralization of sodium hydroxide. It is clear from the titration data that the sorbent can acquire an overall positive or negative charge depending on pH, which suggests that both positively and negatively charged groups are present in varying concentrations. From the C structure, it seems most likely that, in agreement with our proposed model, two monobasic sites, namely amino and hydroxyl groups, account for the charge rather than one type of dibasic site.[42] Site 1 of the model represents hydroxyl groups on the sorbent surface which is supported by the calculated pK_a value > 9. Site 2 is most likely to represent amino groups where pK_a values of 7 to 9 have been reported for amino groups, and surface pK_a values of 4 to 7 have been reported for amino/carboxyl groups.[43] Site 3 represents the possibility of a carboxyl group in the amide of BC, and a pK_a value of 4 supports the possibility. It is assumed from the graphs that up to pH 7 a charge excess is in the negative region so adsorption is higher at lower pH. When titrated after adsorption of metal ions, the charge excess has increased, and instead of giving a sharp rise, the graph shows a flat region from pH 5 to pH 8 in the neutral range, showing the consumption of metal ions with the charge excess.[44,45]

The pK_a spectra resulting from fitting the data using weighted mean value calculations are shown in Figure S2 and Table 2. Surface pK_a values for site 1 appear in the range 4 to 7 pK_a, which have been reported for amino groups in self-assembled monolayers or protonated amines, and for site 2 in the range 7 to 9 pK_a for amine groups.[46,47] Usually high pK_a sites (∼10) are attributed to phenolic hydroxyl sites. Since both C and BC do not have phenolic protons, it is likely that high pK_a sites are for CH_2OH groups, or for primary or secondary amines which have pK_a values in the range 9 to 11. In summary, for site 1 the pK_a sites that are observed here likely correspond to amino groups in self-assembled monolayers or protonated amines, for site 2 to amines, and for site 3 to hydroxyl or amines.

Conclusions

Grafting of barbital on C improves the equilibrium time for uptake of phenyl, methyl, and inorganic Hg^{2+}. Mercury adsorp-

Table 2. Three-Site Model from pK_a Analysis of C and BC Titration Data by Linear Programming

	ligand class		
	1	2	3
range of pK_a	4.0 to 7.0	7.0 to 9.0	9.7 to 11.0
functional group	self-assembled amine/protonated amine	amine	hydroxyl/amine
	Chitosan		
pK_a	5.533	8.6	10.2
L_T	0.0035	0.0027 mmol·g^{-1}	0.0624 mmol·g^{-1}
total concentration	0.0686 mmol·g^{-1}		
	BC		
pK_a	5.2	7.9	10.2
L_T	0.0809 mmol·g^{-1}	0.03845 mmol·g^{-1}	0.0387 mmol·g^{-1}
total concentration	0.15805 mmol·g^{-1}		

tion to C and BC is strongly pH-dependent. There must be more than one mechanism responsible for mercury removal. Amine and amide groups are involved in binding through complexation, weak van der Waals forces, and electrostatic interactions in C and BC, respectively. BC has more binding affinity than C toward Hg^{2+}, which could be due to a larger total number of functional groups present and covalent bonding. More than 99 % of total mercury was removed within 160 min, suggesting instantaneous binding of mercury on surface sites followed by slower and nonspecific binding to other components. The adsorption process fitted well to the Weber−Morris intraparticle diffusion model. Due to the different nature of the adsorbate−adsorbent system and the low initial metal ion concentration used, comparison with other adsorbents is not possible. Speciation was achieved by sequentially eluting inorganic, methyl, and phenyl Hg^{2+} using 0.1 N $HClO_4$, 0.015 N NaCl, and 0.05 N EDTA, respectively.

Acknowledgment

The authors thank Dr. Scott Smith, Department of Chemistry, Wilfrid Laurier University, Department of Applied Mathematics, The M. S. University of Baroda, for Matlab programming, and Department of Chemistry, The M. S. University of Baroda, for laboratory facilities.

Supporting Information Available:

Preparation scheme for C and BC (Scheme S1). Effect of parameters on % uptake of different forms of mercury (Table S1). Isothermal and kinetic parameters (Table S2). Hg 4f spectra of metal-loaded C and BC (Figure S1). pK_a spectra determined by linear programming analysis (Figure S3). This material is available free of charge via the Internet at http://pubs.acs.org.

Literature Cited

(1) Krishnan, K. A.; Anirudhan, T. S. Removal of mercury (II) from aqueous solutions and chlor alkali industry effluents by steam-activated and sulphurised-activated carbons prepared by bagasse pith: Kinetics and equilibrium studies. *J. Hazard. Mater.* **2002**, *92*, 161.
(2) Namasivayam, C.; Periasamy, K. Bicarbonatetreated peanut hull carbon for mercury (II) removal from aqueous solutions. *Water Res.* **1993**, *27*, 1663.
(3) Kamko, K. Dynamic Hg (II) adsorption characterization of iron-oxide-dispersed activated carbon fibres. *Carbon* **1988**, *26*, 903.
(4) Knocke, W. R.; Homphil, L. H. Mercury (II) sorption by waste rubber. *Water Res.* **1981**, *15*, 275.
(5) Kumar, P.; Dara, S. S. Binding heavy metal ions with polymerised onion skin. *J. Polym. Sci.* **1981**, *19*, 397.
(6) Raji, C.; Anirudhan, T. S. Removal of Hg(II) from aqueous solution by sorption on polymerised sawdust. *Ind. J. Chem. Tech.* **1996**, *3*, 49.
(7) Navarvo, R. R.; Sumi, K.; Fugir, N.; Matsumuru, M. Mercury removal from waste water using porous cellulose camer modified with polyethylene amine. *Water Res.* **1996**, *30*, 2488.
(8) Sanchez, P. M.; Utrialla, R. Adsorbent−adsorbate interactions in the adsorption of Cd(II) and Hg(II) on ozonized activated carbons. *Environ. Sci. Technol.* **2002**, *36*, 3850–854.
(9) Shan, H. Y.; Mc Kay, G. Kinetic models for the sorption of dye from aqueous solution by wood. *Ind. Chem. Eng.* **1998**, *76B*, 183–191.
(10) Muzzarelli, R. A. A.; Rocchetti, R. The use of chitosan columns for the removal of mercury from waters. *J. Chromatogr., A* **1974**, *96*, 115–121.
(11) Merrifield, J. D.; Davids, W. G.; MacRae, J. D.; Amirbahman, A. Uptake of mercury by thiol grafted chitosan gel beads. *Water Res.* **2004**, *38*, 3132–3138.
(12) Zhang, A.; Xiang, J.; Sun, L.; Hu, S.; Li, P.; Shi, J.; Fu, P.; Su, S. Preparation, Characterization, and Application of Modified Chitosan Sorbents for Elemental Mercury Removal. *Ind. Eng. Chem. Res.* **2009**, *48*, 4980–4989.
(13) Vieira, R. S.; Beppu, M. M. Mercury ion recovery using natural and cross-linked chitosan membranes. *Adsorption* **2005**, *11*, 731–736.
(14) Oshita, K.; Oshima, M.; Gao, Y. H.; Lee, K. H.; Motomizu, S. Adsorption behavior of mercury and precious metals on cross-linked chitosan and the removal of ultra trace amounts of mercury in concentrated hydrochloric acid by a column treatment with cross-linked chitosan. *Anal. Sci.* **2002**, *18*, 1121–1125.
(15) Choong, J. Mercury ion removal using a packed bed column with granular aminated chitosan. *J. Microbiol. Biotechnol.* **2005**, *15*, 497–501.
(16) Choong, J.; Holl, W. H. Chemical modification of chitosan and equilibrium study of mercury ion removal. *Water Res.* **2003**, *37*, 4770–4780.
(17) Arguelles, W. M.; Peniche, C. C. Preparation and characterization of mercaptan derivative of chitosan for the removal of mercury from brines. *Appl. Macromol. Chem. Phys./Angew. Makromol. Chem.* **1993**, *207*, 1–8.
(18) Peniche, C. C.; Alvarez, L. W.; Arguelles, W. M. The adsorption of mercuric ions by chitosan. *J. Appl. Polym. Sci.* **2003**, *46*, 1147–1150.
(19) Muzzarelli, R. A. A.; Antonio, I. Methyl mercury acetate removal from waters by chromatography on chelating polymers. *Water, Air Soil Pollut.* **1971**, *1*, 65–71.
(20) Karol, C.; Guibal, E.; Francisco, P.; Ly, M.; Holger, M. Mercury Sorption on Chitosan. *Adv. Mater. Res.* **2007**, *20−21*, 635–638.
(21) Gadd, G. M. Biosorption. *Chem. Ind.* **1990**, *13*, 421–426.
(22) Nan, L.; Renbi, B.; Changkun, L. Enhanced and Selective Adsorption of Mercury Ions on Chitosan Beads Grafted with Polyacrylamide via Surface-Initiated Atom Transfer Radical Polymerization. *Langmuir* **2005**, *21*, 11780–11787.
(23) Guibal, E. Metal-Anion Sorption by Chitosan Beads: Equilibrium and Kinetic Studies. *Ind. Eng. Chem. Res.* **1998**, *37*, 1454–1463.
(24) Li, J.; Renbi, B. Mechanisms of Lead Adsorption on Chitosan/PVA Hydrogel Beads. *Langmuir* **2002**, *18*, 9765–9770.
(25) Padmaja, P. Concentration, separation and determination of trace amounts of Hg. Ph.D. Thesis, IIT Madras, 1994.
(26) Curry, A. S. Rapid quantitative Barbiturate estimation. *J. Med. Br.* **1964**, 354.
(27) Chattopadhyay, D. K.; Sreedhar, B.; Kothapalli, V. S. N. R. Effect of chain extender on phase mixing and coating properties of polyureathane Ureas. *Ind. Eng. Chem. Res.* **2005**, *44*, 1772–1779.
(28) Chen, J. P.; Yang, L. Study of a Heavy Metal Biosorption onto Raw and Chemically Modified Sargassum sp. via Spectroscopic and Modeling Analysis. *Langmuir* **2006**, *22*, 8906–8914.
(29) Brassard, P.; Kramer, J. R.; Collins, P. V. Binding site analysis using linear programming. *Environ. Sci. Technol.* **1990**, *24*, 195–2001.
(30) Cox, J. S.; Smith, D. S.; Warren, L. A.; Ferris, F. G. Characterizing heterogeneous Bacterial surface functional groups using discrete affinity spectra for proton binding. *Environ. Sci. Technol.* **1999**, *33*, 4514–5421.
(31) Dittrich, M.; Sibler, S. Influence of H^+ and Calcium Ions on Surface Functional Groups of Synechococcus PCC 7942 Cells. *Langmuir* **2006**, *22*, 5435–5442.
(32) Sokolov, I.; Smith, D. S.; Henderson, G. S.; Gorby, Y. A.; Ferris, F. G. Cell Surface Electrochemical Heterogeneity of the Fe(III)-Reducing Bacteria *Shewanella putrefaciens*. *Environ. Sci. Technol.* **2001**, *35*, 341–347.
(33) Ahuja, P.; Gupta, R.; Saxena, B. K. Zn^{+2} biosorption by Oscillatoria anguistissima. *Process Biochem.* **1999**, *34*, 77.
(34) Gregory, L. R.; Tzu-Yang, H. Synthesis of Porous-Magnetic Chitosan Beads for Removal of Cadmium Ions from Waste Water. *Ind. Eng. Chem. Res.* **1993**, *32*, 2170–2178.
(35) Aldor, T.; Fourest, E.; Volesky, B. Desorption of cadmium from algal biosorbents. *J. Chem. Eng.* **1995**, *73* (1995), 516–522.

(36) Hasan, S.; Krishnaiah, A.; Ghosh, T. K.; Viswanath, D. S. Adsorption of divalent cadmium Cd (II) from aqueous solutions onto chitosan coated perlite beads. *Ind. Eng. Chem. Res.* **2006**, *45*, 5066–5077.
(37) Guibal, E.; Milot, C.; Eterradossi, O.; Gauffier, C.; Domard, A. Study of molybdate ions sorption on chitosan gel beads by different spectrometric analysis. *Int. J. Biol. Macromol.* **1999**, *24*, 49–59.
(38) Huston, N. D.; Attwood, B. C.; Scheckel, K. G. XAS and XPS Characterization of Mercury Binding on Brominated Activated Carbon. *Environ. Sci. Technol.* **2007**, *41*, 1747–1752.
(39) Behra, P.; Gissinger, P. B.; Alnot, M.; Revel, R.; Ehrhardt, J. J. XPS and XAS Study of the Sorption of Hg(II) onto Pyrite. *Langmuir* **2001**, *17*, 3970–3979.
(40) Dittrich, M.; Sibler, S. Cell surface groups of two picocyanobacteria strains studied by zeta potential investigations, potentiometric titration, and infrared spectroscopy. *J. Colloid Interface Sci.* **2005**, *286*, 487–495.
(41) Wang, B.; Oleschuk, R. D.; Horton, J. H. Chemical force titration of amine and sulfonic acid modified poly-(dimethyl siloxane). *Langmuir* **2005**, *21*, 1290–1298.
(42) Leone, L.; Ferri, D.; Manfredi, C.; Persson, P.; Shchukarev, A.; Sjberg, S.; Loring, J. Modeling the Acid-Base Properties of Bacterial Surfaces: A Combined Spectroscopic and Potentiometric Study of the Gram-Positive Bacterium *Bacillus subtilis*. *Environ. Sci. Technol.* **2007**, *41*, 6465–6471.
(43) Guin, V.; Spadini, L.; Sarret, G.; Muris, M.; Delolme, C.; Gaudet, J. P.; Martins, J. M. F. Zinc Sorption to Three Gram-Negative Bacteria: Combined Titration, Modeling, and EXAFS Study. *Environ. Sci. Technol.* **2006**, *40* (6), 1806–1813.
(44) Fonglim, S.; Mingjheng, Y.; Wenzou, S.; Chen, J. P. Characterization of Copper Adsorption onto an Alginate Encapsulated Magnetic Sorbent by a Combined FTIR, XPS, and Mathematical Modeling Study. *Environ. Sci. Technol.* **2008**, *42*, 2551–2556.
(45) Ojeda, J. J.; Gonzlez, M. E. R.; Bachmann, R. T.; Edyvean, R. G. J.; Banwart, S. A. Characterization of the Cell Surface and Cell Wall Chemistry of Drinking Water Bacteria by Combining XPS, FTIR Spectroscopy, Modeling, and Potentiometric Titrations. *Langmuir* **2008**, *24* (8), 4032–4040.
(46) Nishiyama, K.; Kubo, A.; Ueda, A.; Taniguchi, I. Surface pK_a of amine-terminated self assembled mono layers evaluated by direct observation of counter anion by FT-surface enhanced Raman Spectroscopy. *Chem. Lett.* **2002**, 80–81.
(47) Van Der Vegte, E. W.; Hadiionnou, G. Acid-Base properties and the chemical imaging of surface bound functional groups studied with scanning force microscopy. *J. Phys. Chem. B* **1997**, *101*, 9563−9569.

Received for review March 31, 2010. Accepted August 28, 2010. This work has been funded by the Department of Science and Technology, India.

JE100317T